Journal of Environmental Pollution and Control
Volume 5 | Issue 1
ISSN: 2639-9288

Research Article Open Access

Study on Deactivation Mechanism of Catalytic Oxidation of Formaldehyde Over $Ce_xZr_{1-x}O_y$

Liu X[1], Yang ZL[1], Jia LJ[1], Duan KJ[1], Gao JY[1], Chang Y[2] and Liu TC[*1]

[1]College of Chemistry and Environment, Yunnan Minzu University, Technology Innovation Team of Green Purification Technology for Industrial Waste Gas, Education Department of Yunnan, Kunming, China
[2]Yunnan Technician College, Kunming, China

[*]**Corresponding author:** Liu TC, Ph. D College of Chemistry and Environment,Yunnan Minzu University, Technology Innovation Team of Green Purification Technology for Industrial Waste Gas, Education Department of Yunnan, Kunming, China 650504, Tel: +86-13708893755, E-mail: liutiancheng76@163.com

Citation: Liu X, Yang ZL, Jia LJ, Duan KJ, Gao JY, et al. (2022) Study on Deactivation Mechanism of Catalytic Oxidation of Formaldehyde Over CexZr1-xOy. J Environ Pollut Control 5(1): 102

Received Date: January 26, 2022 **Accepted Date:** February 05, 2022 **Published Date:** February 07, 2022

Abstract

Formaldehyde (HCHO) pollution was eliminated by catalyst effectively. The $Ce_xZr_{1-x}O_y$ catalyst was prepared by coprecipitate method, and its performance of HCHO removal was investigated. The results showed that the HCHO removal rate decreased from 100% to 60.88% when the reaction time was from 24h to 48h.In order to study the deactivation mechanism of the $Ce_xZr_{1-x}O_y$ catalyst,N_2 adsorption and desorption, SEM, EDS, FT-IR, XRD and XPS were used to characterize $Ce_xZr_{1-x}O_y$ after different reaction times. Characterization results showed that the pore structure of $Ce_xZr_{1-x}O_y$ did not change significantly with the extension of reaction time, and $C_6H_9CeO_6$ and $Ce(CO_3)_2$ increased gradually, while the active component Ce^{4+} decreased sharply. Therefore, the production and deposition of products are the main reasons for the deactivation of the $Ce_xZr_{1-x}O_y$ catalyst. The catalytic performance of regenerated $Ce_xZr_{1-x}O_y$ catalyst was tested for 24h, and the results showed that it almost recovered to fresh $Ce_xZr_{1-x}O_y$ catalyst. This provides a reference for the preparation of efficient catalyst for formaldehyde removal.

Keywords: Formaldehyde; $Ce_xZr_{1-x}O_y$; Catalytic Oxidation; Deactivation Mechanism

Highlights: (1) The $Ce_xZr_{1-x}O_y$ catalyst had strong stability for formaldehyde. (2) The catalytic oxidation of formaldehyde produced cerium acetate and cerium carbonate, which deactivated the $Ce_xZr_{1-x}O_y$ catalyst. (3) The deactivated $Ce_xZr_{1-x}O_y$ catalyst had excellent catalytic performance after regeneration.

Introduction

Formaldehyde (HCHO) pollution is caused by the release of building materials, household and daily chemicals, and the combustion of cigarettes and fuels [1]. The long-term exposure in formaldehyde environment could cause chronic poisoning, and even lead to leukemia, cancer and other serious diseases [2]. For formaldehyde pollution, researchers at home and abroad have developed formaldehyde purification methods to eliminate indoor formaldehyde pollution, which is divided into physical method [3], chemical method [4-6] and biological method [7,8]. Due to physical and biological methods have problems such as limited absorption capacity and time-consuming biological growth, chemical method has become a research focus of formaldehyde removal. For example, Ma et al. [9] improved the catalytic activity of Ag/CeO_2 for HCHO by doping Na. The experimental result showed that the HCHO conversion rate was 30% at room temperature. Rong et al. [10] prepared a mesh structure 3D-MnO_2 to remove HCHO with a conversion rate of 45%. Fang et al. [11] prepared MnO_x/AC methanol catalyst for catalytic oxidation of HCHO. The study showed that the HCHO removal rate was basically maintained at 100% within 1000 min. Although these catalysts have achieved good results in removing HCHO, they all faced the problem that the activity of the catalyst decreased with the progress of the reaction. Therefore, it is an urgent scientific research project to find a highly stable catalyst for formaldehyde removal.

Ce, as a cheap and widely used lanthanide element, has special oxygen storage and release functions. ZrO_2 has abundant surface oxygen vacancy and strong ion exchange ability, which can show unique catalytic effect when interacting with some active components in the system. Using Ce load in ZrO_2 will have better oxygen storage capacity and redox capacity. For example, Fu QJ [12] prepared Pt/ $Ce_{0.5}Zr_{0.5}O_2$ catalyst and investigated its catalytic combustion performance on C_2H_6. The results showed that Pt/ $Ce_{0.5}Zr_{0.5}O_2$ had excellent activity on C_2H_6 combustion. $Ce_xZr_{1-x}O_y$ prepared by Ding YQ [13] showed high activity for CO oxidation and CH_4 combustion. Gao X [14] prepared $Ce_{0.7}Zr_{0.3}O_2$ for selective catalytic reduction of NO, and the conversion rate reached 100%. It can be seen from the above that Ce/Zr is a catalyst with excellent performance, but its application in catalytic oxidation of formaldehyde is rarely reported.

The $Ce_xZr_{1-x}O_y$ catalyst was prepared by co-precipitation method, and its catalytic performance for removing HCHO was investigated. Through the characterization of $Ce_xZr_{1-x}O_y$ at different reaction times, the reasons for deactivation were analyzed, which provided a reference for the development of the preparation of highly stable catalysts.

Materials and Method

Materials

Cerium nitrate ($Ce(NO_3)_3{\cdot}6H_2O$) and zirconium nitrate ($Zr(NO_3)_4{\cdot}5H_2O$) were purchased from Macklin.Hydrazine hydrate ($N_2H_4{\cdot}H_2O$) was purchased from Tianjin Fengchuan Chemical Reagent Co., LTD.

Method

The $Ce_xZr_{1-x}O_y$ catalyst was prepared by co-precipitation method [15,16]. First, $Ce(NO_3)_3{\cdot}6H_2O$ and $Zr(NO_3)_4{\cdot}5H_2O$ were dissolved with an appropriate amount of distilled water in a beaker, and got a mixed solution (the molar ratio of Ce to Zr was 4). Then, added slowly $N_2H_4{\cdot}H_2O$ solution and adjusted the pH value of the mixed solution, prepared the $Ce_xZr_{1-x}O_y$ precipitate. After aging for 4h, the precipitate was filtered, washed and dried into the $Ce_xZr_{1-x}O_y$ crystallization [17]. Finally, the crystallization was calcined at 500 °C for 4h to obtain the $Ce_xZr_{1-x}O_y$ catalyst.

Catalyst characterization

The crystal structure of samples was detected by X-ray powder diffractometer (XRD, Bruker D8 Advance, Germany), using CuKα radiation, The intensity data were collected in a 2θ from 10° to 80°.

N_2 adsorption was determined by the analyzer (Michael 2460, USA). The operating condition was controlled as follows: the samples were purified and degassed at 200 °C for 3h and analyzed by static adsorption method under N_2 atmosphere at 77K (liquid nitrogen). Specific surface area was calculated by BET equation.

The chemical state of element was determined by X-ray photoelectron spectroscopy (XPS,Thermo Scientific K-Alpha,USA). The radiation source was AlKα, the operating voltage was 12kV, and the binding energy was calibrated with internal standard carbon 1s peak (E_b= 284.80eV) with an accuracy of ±0.2eV.

The surface morphology of the catalyst was observed using a scanning electron microscope (SEM, Gemini300, Germany). Spectrometer (EDS, Oxford X-MAX,UK) was used for energy spectrum analysis. The acceleration voltage was 30kV, and the samples were dispersed with ethanol, dried, and sprayed with platinum.

The product functional groups on the surface of the catalyst were detected by the infrared spectrometer (FT-IR,Thermerfeld Nicolet iS20,USA).

Catalyst evaluation

The experimental process is shown in Figure 1. The HCHO catalytic oxidation reaction was operated in a fixed bed reactor under atmospheric pressure, 0.2g $Ce_xZr_{1-x}O_y$ catalyst and 50g SiO_2 were loaded in the reactor. The volume fraction of each gas was 20% O_2, 60% HCHO, and N_2 as the equilibrium gas. The concentration of HCHO was determined by spectrophotometry [18].

$$\text{Conversion of HCHO} = \frac{[HCHO]i - [HCHO]f}{[HCHO]i} \times 100\% \quad (1)$$

where [HCHO]i (mg·L^{-1}) is the initial concentration of HCHO before the test started, and [HCHO]f (mg·L^{-1}) is the final concentration of HCHO at the end of the test.

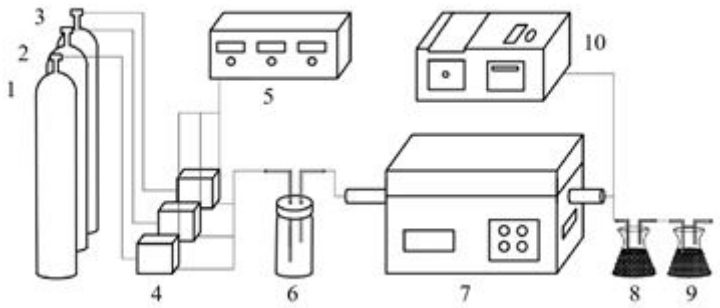

Figure 1: Experimental flow chart (1-HCHO cylinder; 2-O_2 cylinder; 3-N_2 cylinder; 4-Mass flow controller; 5-Mass flow control box; 6-Woulff's bottle; 7-Tube furnaces; 8-NaOH solution; 9-SiO_2; 10-Spectrophotometer)

Results and Discussions

Catalytic performance of $Ce_xZr_{1-x}O_y$

To investigate the stability of the $Ce_xZr_{1-x}O_y$ catalyst, the catalytic oxidation reaction lasted for 48h, and the results are shown in Figure 2. When the catalytic oxidation experiment was carried out for 12 hours, the HCHO removal rate remained at 100%. Even after 24h reaction, formaldehyde removal rate could reach 99.67%, closed to complete degradation. The reason why the $Ce_xZr_{1-x}O_y$ catalyst had such a high catalytic effect is that it has loose and porous morphology and abundant reaction sites. When the reaction lasted for 36h, the catalyst deactivation led to a significant decrease in HCHO degradation rate, but it still remained above 90%. With the progress of the reaction, the HCHO removal rate decreased to 78.29% at 42h. Until the end of catalytic oxidation, the HCHO removal rate was 60.88%. In order to improve the accuracy of the data, the experiment was repeated 5 times under the same conditions, and the results showed a high recurrence rate.

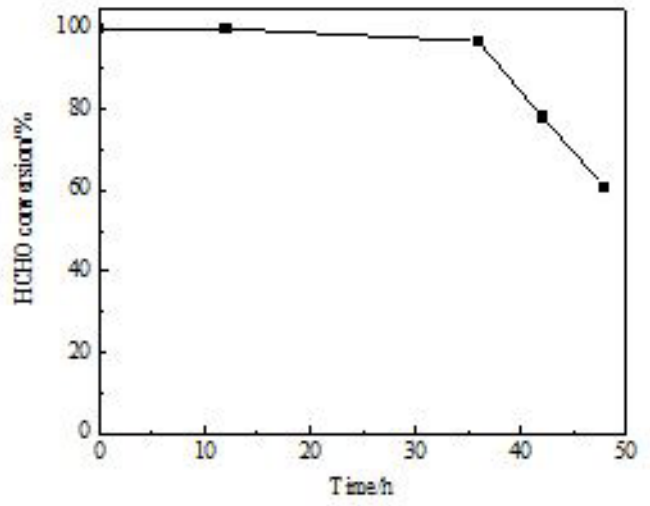

Figure 2: Stability test of $Ce_xZr_{1-x}O_y$

The deactivation mechanism of $Ce_xZr_{1-x}O_y$

Morphology structure analysis

N_2 adsorption and desorption were tested on the deactivated $Ce_xZr_{1-x}O_y$ to explore the reasons for the decrease of catalyst activity. Table 1 shows the physical properties of $Ce_xZr_{1-x}O_y$ after reaction at 0h, 12h, 24h and 48h. It can be seen that with the extension of reaction time, the specific surface area, pore volume and average pore size of $Ce_xZr_{1-x}O_y$ tended to decrease, but the decrease rate tended to small. This phenomenon could be attributed to the formation of some solid species with higher SSA into the oxides [19]. In conclusion, the deactivation of $Ce_xZr_{1-x}O_y$ was not caused by changes in specific surface area and pore structure, but was probably related to the blockage of pores by solid species

Sample	$S_{BET}/m^2 \cdot g^{-1}$	$V_{Pore}/cm^3 \cdot g^{-1}$	D_{Pore}/nm
$Ce_xZr_{1-x}O_y$-0h	59.610	0.112	6.405
$Ce_xZr_{1-x}O_y$-24h	52.160	0.109	5.632
$Ce_xZr_{1-x}O_y$-42h	43.003	0.103	4.254
$Ce_xZr_{1-x}O_y$-48h	42.737	0.101	4.143

Table 1: Physical properties of $Ce_xZr_{1-x}O_y$

SEM results of deactivated $Ce_xZr_{1-x}O_y$ and fresh $Ce_xZr_{1-x}O_y$ are shown in Figure 3. Figure 3(a) shows the morphology of fresh $Ce_xZr_{1-x}O_y$, and its surface was smooth and flat without covering of particles. However, a large number of particles were deposited on the surface of deactivated $Ce_xZr_{1-x}O_y$, as shown in Figure 3(b),Figure 3(c) and Figure 3(d). With the extension of reaction time, more and more particles were deposited, and even dense structures formed by particle agglomeration appeared. Figure 4 shows the EDS test results of $Ce_xZr_{1-x}O_y$ after the reaction. The atomic proportion of oxygen (O), carbon (C) and cerium (Ce) were much higher than that of other elements, among which carbon element might be brought by product CO_2. Thus speculate that surface particle deposition is one of the causes of $Ce_xZr_{1-x}O_y$ deactivation, and the particles may be mainly composed of O, C and Ce elements.

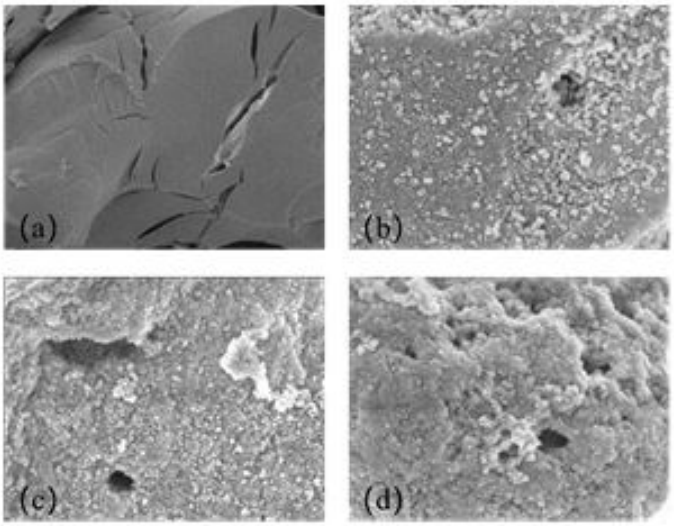

Figure 3: SEM images of $Ce_xZr_{1-x}O_y$ after (a)0h,(b)24h,(c)42h,(d)48h reaction

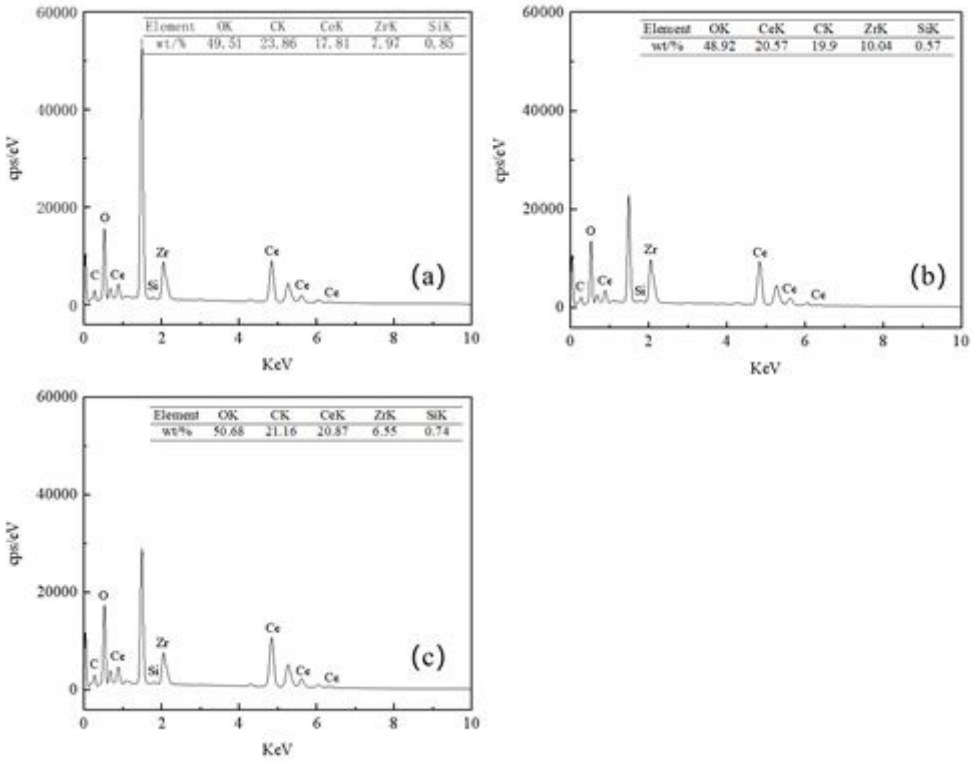

Figure 4: EDS pattern of $Ce_xZr_{1-x}O_y$ after (a)24h,(b)42h,(c)48h reaction

Phase composition analysis

$Ce_xZr_{1-x}O_y$ was determined by Fourier transform infrared spectrometer. Firstly, as can be seen from Figure 5, absorption peaks appeared at 3381.71cm^{-1}, 3377.42cm^{-1}, 3378.97cm^{-1} and 3377.90cm^{-1}, which neared 3300cm^{-1},indicating OH group [20,21]. Fresh $Ce_xZr_{1-x}O_y$ peak had sharp shape without interference and it can infer to be OH group of unbound water. It may be that the low coordination O^{2-} anions present on the basic support promoted the dissociation of water and produced OH group [22-24]. It can be used to supplement the OH group consumed in the decomposition process of HCHO [25-27]. After the reaction, the OH group absorption peaks of $Ce_xZr_{1-x}O_y$ were wide and scattered, and a series of small peaks appeared in the range of 2700-2500cm^{-1}, which are judged as characteristic peaks of carboxylic acid [28]. The absorption peaks of $Ce_xZr_{1-x}O_y$ after 42-48h reaction were observed at 1564.28cm^{-1} and 1567.96cm^{-1}, which are C=O antisymmetric stretching vibration of carboxylate, while the symmetric stretching vibration of 1440-1360cm^{-1} is weak [29-31]. It can be speculated that HCHO reacted with adsorbed oxygen species to produce formate [32], and then formed a cerium salt of organic acid with cerium. Secondly, the absorption peaks of $Ce_xZr_{1-x}O_y$ after the reaction appeared at 1073.51cm^{-1} and 1080.64cm^{-1}, which are C-O absorption peaks [33]. It is speculated that formaldehyde was catalyzed to generate CO_2 products, which further reacted to form carbonate substances. In conclusion, the catalytic oxidation of formaldehyde by $Ce_xZr_{1-x}O_y$ generates organic acid cerium salts and carbonate particles. This conclusion is consistent with EDS analysis.

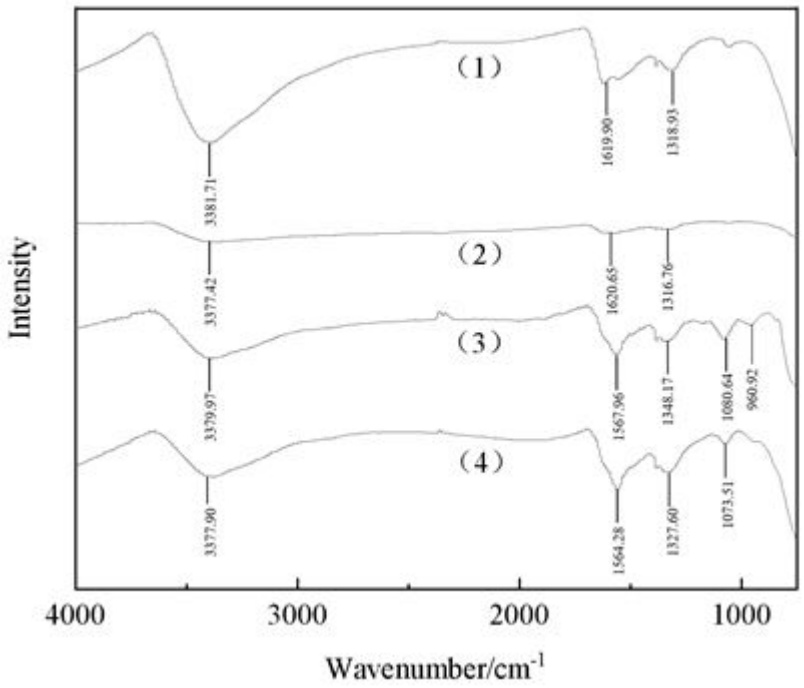

Figure 5: Infrared pattern of $Ce_xZr_{1-x}O_y$ after (1)0h,(2)24h,(3)42h,(4)48h reaction

Figure 6 shows the $Ce_xZr_{1-x}O_y$ XRD pattern of different reaction times. For $Ce_xZr_{1-x}O_y$ before the reaction, the diffraction peaks at 2θ of 28.87 °, 33.47 °, 48.05°, 57.01°, 59.85°, 70.36° were attributed to the diffraction peaks of $Ce_xZr_{1-x}O_y$(JCPDS 28-0271). At the same time, the characteristic peaks of CeO_2 and ZrO_2 did not appear in the XRD pattern, indicating that the active component were evenly distributed on the surface of $Ce_xZr_{1-x}O_y$ [34]. The diffraction peak intensity of $Ce_xZr_{1-x}O_y$ (24h) increased, which may be due to the overlapping effect of particles on crystals. With the progress of the reaction (42-48h), the diffraction peak of $Ce_xZr_{1-x}O_y$ faded rapidly and partially disappeared, indicating that Ce was further oxidized to $Ce(CO_3)_2$ and $C_6H_9CeO_6$ in the reaction process, which is consistent with the infrared analysis results.At the same time, the diffraction peak intensity of $Ce(CO_3)_2$ and $C_6H_9CeO_6$ slightly increased, indicating that their grain size gradually increased with the progress of the reaction, that is, $Ce(CO_3)_2$ and $C_6H_9CeO_6$ on the surface of $Ce_xZr_{1-x}O_y$ appeared agglomeration phenomenon. It is consistent with the SEM results. In conclusion, cerium acetate and cerium carbonate accumulated in the $Ce_xZr_{1-x}O_y$ channel, hindering the contact between HCHO and the active component and weakening the activity of $Ce_xZr_{1-x}O_y$.

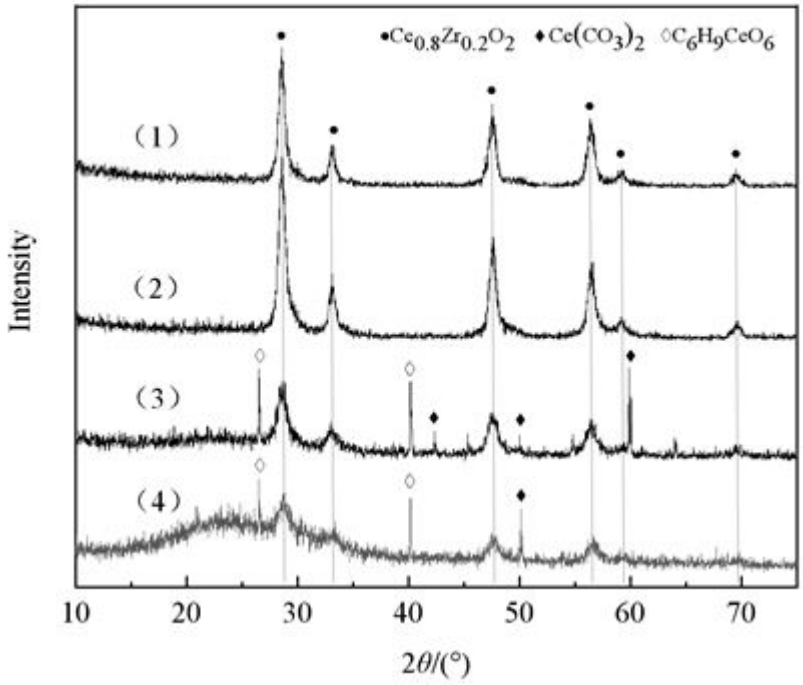

Figure 6: XRD pattern of $Ce_xZr_{1-x}O_y$ after (1)0h,(2)24h,(3)42h,(4)48h reaction

Active component analysis

XPS was used to analyze the content and morphology of $Ce_xZr_{1-x}O_y$ element. In Figure 7,U and V correspond to the spin splitting orbits of Ce $3d_{3/2}$ and Ce $3d_{5/2}$ respectively. The peaks located at 897.82eV (V_4), 888.28eV (V_3),881.69eV (V_1),916.08eV (U_4),906.58eV (U_3),900.28eV (U_1) belong to Ce^{4+}.The peaks located at 883.9eV (V_2) and 902.34eV (U_2) belong to Ce^{3+} [35]. It created a charge imbalance, forming some oxygen vacancies and unsaturated chemical bonds [36]. The existence of Ce^{3+} is due to the tiny particle size of cerium oxide, changes in the coordination of the Ce atoms, or changes in net charge caused by its shared anion with ZrO_2 [37]. It can be obtained from Figure that the peak located at 534.1 and 529.5 eV, the former belong to the adsorbed oxygen (O_a) or surface hydroxyl oxygen of the catalyst, and the latter belong to the lattice oxygen (O_b) in the catalyst [38]. Surface hydroxyl oxygen can not only provide reaction sites for hydrogen bond adsorption of formaldehyde molecules, but also accelerate the catalytic oxidation of HCHO by using hydroxyl oxidation properties [39].

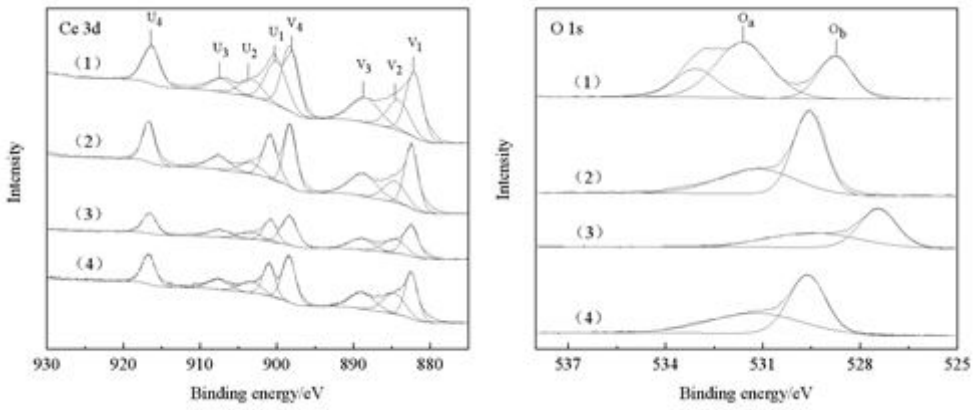

Figure 7: XPS spectra of $Ce_xZr_{1-x}O_y$ after (1)0h,(2)24h,(3)42h,(4)48h reaction

Through semi-quantitative calculation of peak area, the molar ratio of Ce^{4+} and O_a can be obtained, and the results are listed in Table 2. The content of Ce^{4+} decreased with the extension of reaction time, indicating that Ce^{4+} was involved in the catalytic oxidation reaction as the active component. At the same time, the O_a also decreased with Ce^{4+} concentration, indicating that O_a was consumed in the catalytic reaction. It can be concluded that Ce^{4+}, as the active component, oxidizes HCHO to CO_2 and H_2O, and turn itself into Ce^{3+}, while Ce^{3+} is oxidized to Ce^{4+} by O_a to supplement the active component and maintain high catalytic activity of $Ce_xZr_{1-x}O_y$.

Reaction time	$\frac{n(Ce^{4+})}{n(Ce^{3+}+Ce^{4+})}(\%)$	$\frac{n(O_a)}{n(O_a+O_b)}(\%)$
$Ce_xZr_{1-x}O_y$-0h	93.72	85.3
$Ce_xZr_{1-x}O_y$-24h	91.27	25.28
$Ce_xZr_{1-x}O_y$-42h	90.16	22.81
$Ce_xZr_{1-x}O_y$-48h	86.18	21.06

Table 2: Results of the XPS analysis for $Ce_xZr_{1-x}O_y$

Combined with SEM, EDS, FT-IR and XRD characterization analysis, it is concluded that the formate reacted with Ce to produce $C_6H_9CeO_6$,CO_2 reacted with Ce to transform into $Ce(CO_3)_2$ in the catalytic oxidation of HCHO by $Ce_xZr_{1-x}O_y$.These production not only occupied the active site, but also consumed Ce^{4+},which broke the benign cycle of "supplement-consumption-supplement" of active components. The above reasons results in the decreased activity of $Ce_xZr_{1-x}O_y$.

Catalytic performance of calcined regenerated $Ce_xZr_{1-x}O_y$

To confirm that products deposition is the main cause of $Ce_xZr_{1-x}O_y$ deactivation, the deactivated $Ce_xZr_{1-x}O_y$ was collected and calcined at 700 °C for 4h.The regenerated $Ce_xZr_{1-x}O_y$ was characterized by IR, XRD and SEM.

As shown in Figure 8, C-O absorption peaks of carbonate were not observed in infrared spectrum of the regenerated $Ce_xZr_{1-x}O_y$. The carboxylic acid characteristic peak of the regenerated $Ce_xZr_{1-x}O_y$ was also not as obvious as that after the reaction. These indicating that $Ce(CO_3)_2$ and $C_6H_9CeO_6$ had been decomposed after calcining, which is also confirmed in the XRD pattern (Figure 9).As can be seen from Figure 10,only a few particles remained on the surface of the regenerated $Ce_xZr_{1-x}O_y$.According to the XRD pattern, these particles might be SiO_2 that was not separated during the collection of deactivated $Ce_xZr_{1-x}O_y$.From the characterization results, there is no significant difference between the calcined regenerated $Ce_xZr_{1-x}O_y$ and the fresh $Ce_xZr_{1-x}O_y$.

For further verify that the catalytic activity was recovered after the decomposition of the product. The catalytic performance of the regenerated $Ce_xZr_{1-x}O_y$ was tested for 24h and the results are shown in Figure 11. Within 12h of the reaction, the HCHO removal rate of 100% was basically maintained. With the progress of the reaction, the HCHO removal rate was slightly reduced to 98.67% at 24h. After testing, the HCHO removal rate of regenerated $Ce_xZr_{1-x}O_y$ can basically reach the fresh $Ce_xZr_{1-x}O_y$. These results confirm that the deposition of $Ce(CO_3)_2$ and $C_6H_9CeO_6$ is the main cause of $Ce_xZr_{1-x}O_y$ deactivation.

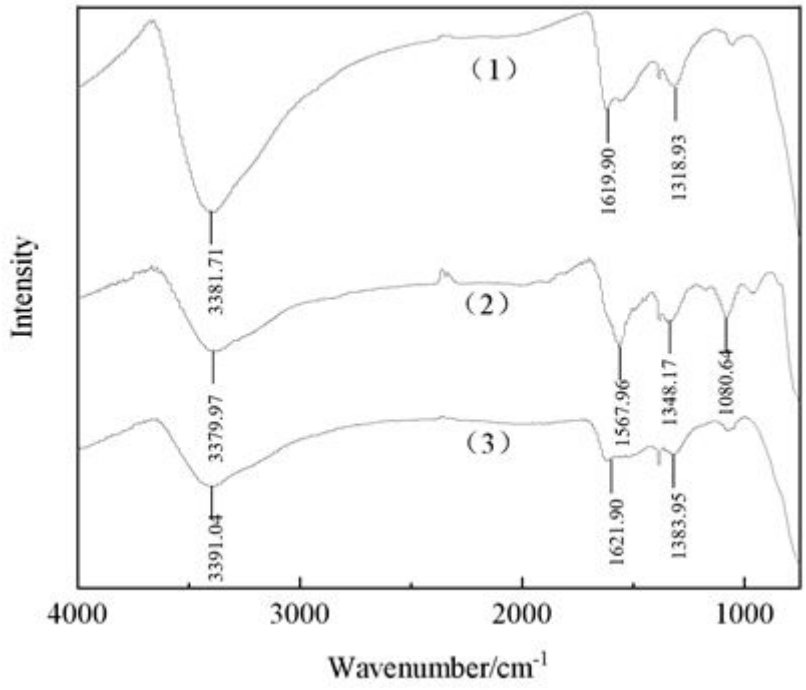

Figure 8: Infrared pattern of (1)fresh, (2)deactivated, (3)regenerated $Ce_xZr_{1-x}O_y$

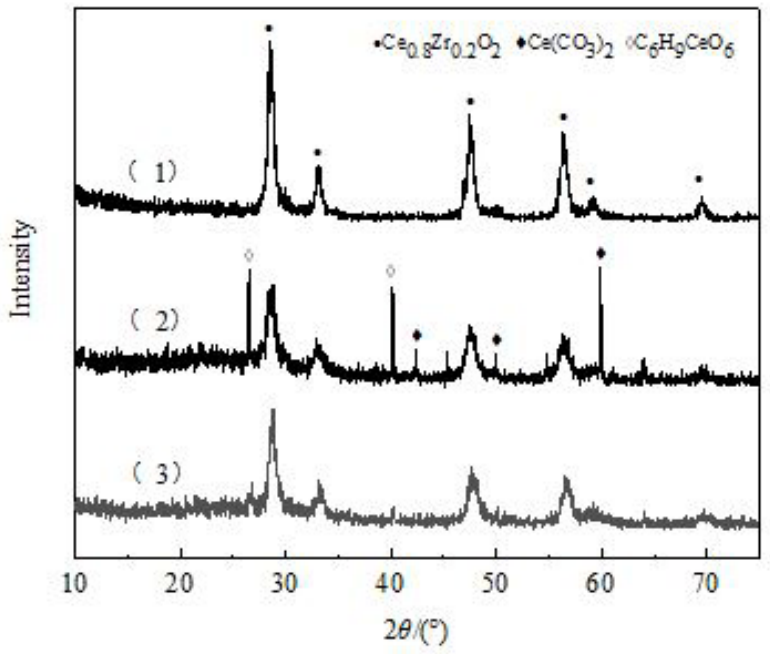

Figure 9: XRD pattern of (1)fresh, (2)deactivated, (3)regenerated $Ce_xZr_{1-x}O_y$

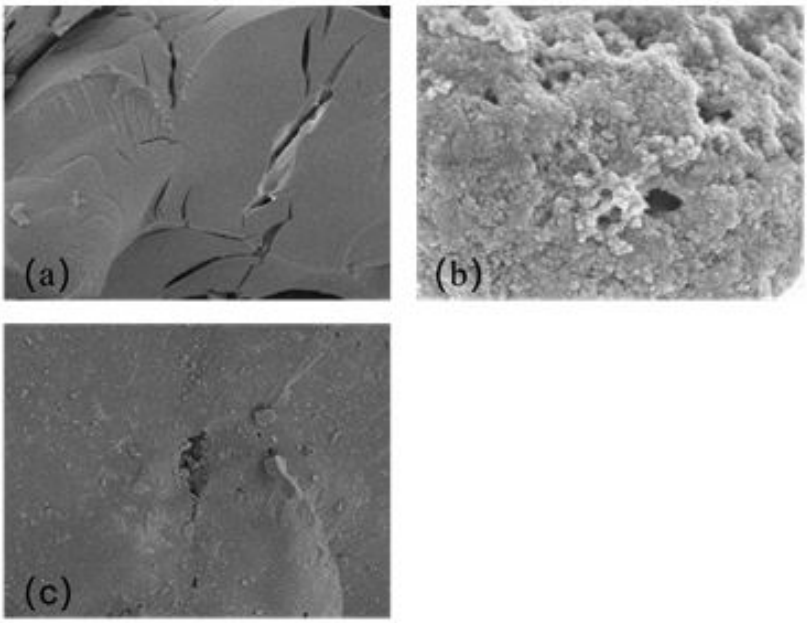

Figure 10: SEM images of (a)fresh, (b)deactivated, (c)regenerated $Ce_xZr_{1-x}O_y$

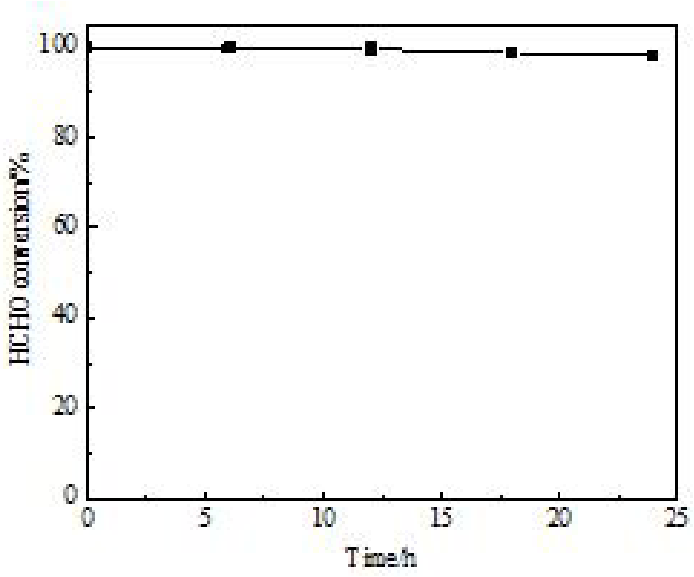

Figure 11: Stability test of regenerated $Ce_xZr_{1-x}O_y$

Conclusions

The $Ce_xZr_{1-x}O_y$ catalyst had a good catalytic oxidation effect on HCHO removal, and HCHO removal rate was close to 100% within 24h of reaction. Characterization results of deactivated $Ce_xZr_{1-x}O_y$ catalyst showed that during the HCHO removal, the products of $Ce(CO_3)_2$ and $C_6H_9CeO_6$ blocked the pore, occupied the reaction site, consumed the active component Ce^{4+}, and led to the deactivation of the $Ce_xZr_{1-x}O_y$ catalyst.

Funding

Financial support from the National Natural Science Foundation of China (51568068), young and middle-aged academic and technical leaders reserve talent project of yunnan (cn) (202105AC160054) are gratefully acknowledged.

Conflicts of Interest

The authors declare no conflicts of interest.

References

1. He C, Cheng J, Zhang X, Douthwaite M, Pattisson S, et al. (2019) Recent advances in the catalytic oxidation of volatile organic compounds:a review based on pollutant sorts and sources. Chem Rev 119: 4471-568.

2. Zhang X, Zhao Y, Song J, Yang X, Zhang J, et al. (2018) Differential health effects of constant versus intermittent exposure to formaldehyde in mice: Implications for building ventilation strategies. Environ Sci Technol 52: 1551-60.

3. Johnson DL, Lynch RA, Floyd EL, Wang J, Bartelsa JN (2018) Indoor air quality in classrooms: Environmental measures and effective ventilation rate modeling in urban elementary schools. Build Environ 136: 185-97.

4. Niu S, Yan HX (2015) Novel silicone-based polymer containing active methylene designed for the removal of indoor formaldehyde. J Hazard Mater 287: 259-67.

5. Russell HS, Bonomaully J, Bossi R, Hofmann MEG, Knap HC, et al. (2020) Novel materials for combined nitrogen dioxide and formaldehyde pollution control under ambient conditions. Catal 10: 1040.

6. Shi YY, Qiao ZW, Liu ZL, Zuo JL (2019) Cerium doped Pt/TiO2 for catalytic oxidation of low concentration formaldehyde at room temperature. Catal Lett 149: 1319-25.

7. Shao YH, Wang YX, Zhao R, Chen JM, Zhang FM, et al. (2020) Biotechnology progress for removal of indoor gaseous formaldehyde. Appl Microbiol Biotechnol 104: 3715-27.

8. Goli A, Talaiekhozani A, Eshtiaghi N, Chisti Y, Aramesh R, et al. (2017) Biotreatment of formaldehyde-contaminated air in a trickle bed bioreactor. Desalination Water Treat 93: 83-92.

9. Ma L, Seo CY, Chen XY, Li JH, Schwank WJ (2018) Sodium-promoted Ag/CeO2 nanospheres for catalytic oxidation of formaldehyde. Chem Eng J 350: 419-28.

10. Rong SP, Zhang PY, Yang YJ, Zhu L, Wang JL, et al. (2017) MnO2 framework for instantaneous mineralization of carcinogenic airborne formaldehyde at room temperature. ACS Catalysis 7: 1057-67.

11. Fang RM, Hang HB, Ji J, He M, Feng QY, et al. (2018) Efficient MnOx supported on coconut shell activated carbon for catalytic oxidation of indoor formaldehyde at room temperature. Chem Eng J 334: 2050-7.

12. Fu QJ, Wang S, Wang T, Xing DF, Yue X, et al. (2022) Insights into the promotion mechanism of ceria-zirconia solid solution to ethane combustion over Pt-based catalysts. J Catal 405: 129-39.

13. Ding YQ, Wang Z, Guo YL, Guo Y, Wang L, et al.(2019)A novel method for the synthesis of CexZr1-xO2 solid solution with high purity of Kappa phase and excellent reactive activity. Catal Today 327: 262-70.

14. Gao X, Zhang S, Du WX, Gong XC, Nguyen TT, et al. (2021) Wood-inspired high-performing hierarchical porous Ce0.7Zr0.3O2 catalyst for low-temperature selective catalytic reduction of NOx by NH3. Ceram Int 47: 29149-61.

15. Lukasz W, Grzegorz N, Stefan J, Maria Z (2021) Influence of Co-precipitation agent on the structure, texture and catalytic activity of Au-CeO2 catalysts in low-temperature oxidation of benzyl alcohol. Catal 11: 641-2.

16. Hori CE, Permana H, Ng KYS, Brenner A, More K, et al. (1998) Thermal stability of oxygen storage properties in a mixed CeO2-ZrO2 system. Appl Catal B Environ 16: 105-17.

17. Nandi M, Talukdar AK (2016) Ceria-zirconia solid solution loaded hierarchical MFI zeolite: An efficient catalyst for solvent free oxidation of ethyl benzene. Arab J Chem 12: 3753-63.

18. The National Health and Family Planning Commission of the People's Republic of China (2014) Examination methods for public places- Part 2 Chemical pollutants, China.

19. Lange J, Price R, Ayoub P, Louis J, Petrus L, et al. (2010) Valeric biofuels: a platform of cellulosic transportation fuels. Angew Chem Int Ed 49: 4479-83.

20. Liu RR, Wang J, Zhang JJ, Xie S, Wang XY, et al. (2017) Honeycomb-like micromesoporous structure TiO2/sepiolite composite for combined chemisorption and photocatalytic elimination of formaldehyde. Microporous Mesoporous Mater 248: 234-45.

21. Dan-Hardi M, Serre C, Frot T, Rozes L, Maurin G, et al. (2009) A new photoactive crystalline highly porous titanium (IV) dicarboxylate. J Am Chem Soc 131: 10857-9.

22. Shabaker JW, Davda RR, Huber GW, Cortright RD, Dumesic JA (2003) Aqueous-phase reforming of methanol and ethylene glycol over alumina-supported platinum catalysts. J Catal 215: 344-52.

23. Davda RR, Shabaker JW, Huber GW, Cortright RD, Dumesic JA (2005) A review of catalytic issues and process conditions for renewable hydrogen and alkanes by aqueousphase reforming of oxygenated hydrocarbons over supported metal catalysts. Appl Catal B Environ 56: 171-86.

24. Huber GW, Davda RR, Shabaker JW, Cortright RD, Dumesic JA (2003) Aqueous-phase reforming of ethylene glycol on silica-supported metal catalysts. Appl Catal B Environ 43: 13-26.

25. Fang RM, Huang HB, Huang WJ, Ji J, Feng QY, et al. (2017) Influence of peracetic acid modification on the physicochemical properties of activated carbon and its performance in the ozone-catalytic oxidation of gaseous benzene. Appl Surf Sci 420: 905-10.

26. Zhang C, Liu F, Zhai Y, Ariga H, Yi N, et al. (2012) Alkali-metal-promoted Pt/TiO2 opens a more effiffifficient pathway to formaldehyde oxidation at ambient temperatures. Angew Chem Int Ed 51: 9628-32.

27. Nie LH, Yu JG, Li XY, Cheng B, Liu G, et al. (2013) Enhanced Performance of NaOH-Modified Pt/TiO2 toward Room Temperature Selective Oxidation of Formaldehyde. Environ Sci Technol 47: 2777-83.

28. Fang RM, Huang HB, Ji J, He M, Feng QY, et al. (2018) Efficient MnOx supported on coconut shell activated carbon for catalytic oxidation of indoor formaldehyde at room temperature. Chem Eng J 334: 2050-7.

29. Suligoj A, Stangar UL, Ristic A, Mazaj M, Verhovsek D, et al. (2016) TiO2-SiO2 films from organic-free colloidal TiO2 anatase nanoparticles as photocatalyst for removal of volatile organic compounds from indoor air. Appl Cat B Environ 184: 119-31.

30. Jin DQ, Xu Q, Yu LY, Hu XY (2015) Photoelectrochemical detection of the herbicide clethodim by using the modified metal-organic framework amino-MIL-125 (Ti)/TiO2. Microchim Acta 182: 1885-92.

31. Petit C, Bandosz TJ (2011) Synthesis, characterization, and ammonia adsorption prop erties of mesoporous metal-organic

framework (MIL(Fe))-graphite oxide compo sites: exploring the limits of materials fabrication. Adv Funct Mater 21: 2108-17.

32. Wang JL, Li J, Jiang CJ, Zhou P, Zhang PY, et al. (2017) The effect of manganese vacancy in birnessite-type MnO2 on room-temperature oxidation of formaldehyde in air. Appl Catal B Environ 204: 147-55.

33. Rong SP, Zhang PY, Wang JL, Liu F, Yang YJ, et al. (2016) Ultrathin manganese dioxide nanosheets for formaldehyde removal and regeneration performance. Chem Eng J 306: 1172-9.

34. Chen AP, Guo HJ, Song YM, Chen P, Lou H (2017) Recyclable CeO2–ZrO2 and CeO2–TiO2 mixed oxides based Pt catalyst for aqueous-phase reforming of the low-boiling fraction of bio-oil. Int J Hydrog Energy 42: 9577-88.

35. Jin QJ, Shen YS, Zhu SM, Liu Q, Li XH, et al. (2016) Effect of praseodymium additive on CeO2 (ZrO2) /TiO2 for selective catalytic reduction of NO by NH3. J Rare Earths 34: 1111-20.

36. Zamar F, Trovarelli, Leitenburg CD, Dolcetti G (1995) Cheminform abstract: CeO2-based solid solutions with the flfluorite structure as novel and effective catalysts for methane combustion. Cheminform 26.

37. Gao X, Jiang Y, Zhong Y, Luo ZY, Cen K (2010) The activity and characterization of CeO2-TiO2 catalysts prepared by the sol-gel method for selective catalytic reduction of NO with NH3. J Hazard Mater 174: 734-9.

38. Wang T, Chen S, Wang HQ, Liu Z, Wu ZB (2017) In-plasma catalytic degradation of toluene over different MnO2 polymorphs study of reaction mechanism. Chinese J Catal 38: 793-804.

39. Huang QQ, Hu Y, Pei Y, Zhang JH, Fu ML (2019) In situ synthesis of TiO2@NH2-MIL-125 composites for use in combined adsorption and photocatalytic degradation of formaldehyde. Appl Catal B Environ 259: 118106.